*31st EPS Conference on Plasma Phys. London, 28 June - 2 July 2004 ECA Vol.**28G**, P-5.107 (2004)*

Magnetic Measurements for MHD Equilibrium Reconstruction in LHD

T. Yamaguchi[1], K.Y. Watanabe[2], S. Sakakibara[2], K. Yamazaki[2], Y. Narushima[2] , K. Narihara[2],
K. Tanaka[2] and LHD Experimental Group[2]

1. The Graduate University for Advanced Studies, Toki 509-5292, Japan

2. National Institute for Fusion Science, Toki 509-5292, Japan

1. Introduction

In helical systems, the characteristics of magnetohydrodynamic (MHD) equilibrium, stability and transport with the high plasma pressure and the large toroidal current are quite different from those in vacuum. Then, it is one of the important issues to establish a method of MHD equilibrium reconstruction consistent with experimental observations. Though magnetic measurements are known to be powerful tools for the MHD equilibrium reconstruction, the MHD equilibrium reconstruction method using magnetic measurements has not established in helical devices. However, the magnetic measurements have a capability to measure the important equilibrium parameters like beta, its profile and the pressure anisotropy[1, 2]. To estimate beta value, two types of magnetic diagnostics, the diamagnetic flux loop and saddle flux loops, are installed in LHD. The diamagnetic flux loop is sensitive to the total plasma energy but it is not sensitive to the pressure profile. On the contrary, saddle flux loops are sensitive to both of them. As another difference, the diamagnetic flux loop measures the diamagnetic current induced by the perpendicular pressure ($p_\perp$), while saddle loops measure Pfirsch-Schlüter (P.S.) current induced by the sum of the perpendicular and parallel pressures ($p_\perp+p_\parallel$). In this paper, we focus the effect of anisotropic beam pressure on the total pressure based on magnetic measurements.

2. Experimental setup

LHD is a heliotron device with L=2 and M=10 super-conducting helical coils and three pairs of poloidal coils[3]. Here L is a pole number and M is the field period of helical coil system. The machine major radius is 3.9 m, and the plasma minor radius is 0.64 m in a typical operation. The diamagnetic loop is installed inside vacuum vessel. The eddy current in structures are measured with Rogowski coils. The current increment of the helical coils and poloidal coils during discharges are also measured. They are used for calibrations of the diamagnetic flux. Saddle loops have been installed along helical coils inside vacuum vessel. Figures 1 and 2 show locations of saddle loops in a top-view and a poloidal cross section. They are not sensitive to the magnetic field from helical coil currents and eddy currents in structures, because they flow in the parallel direction of them. In LHD, there are 24 saddle loops whose toroidal and poloidal angles are different. The saddle loops whose positions are top or bottom of plasmas are used for this study because they are suitable to measure magnetic field from P.S. current.

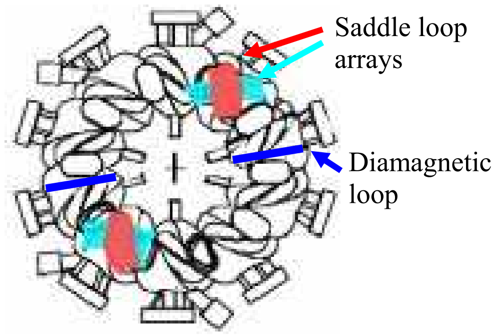

Fig.1 The location of saddle flux loops and diamagnetic loops.

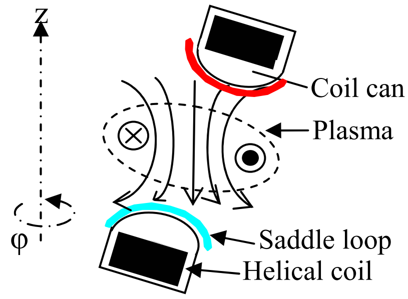

Fig.2 Saddle flux loops location and P.S. current.

3. Equilibrium analyses

The fluxes of magnetic diagnostics are estimated by using 3-D MHD equilibrium analysis code VMEC[4] and DIAGNO[5] under the asummption of isotropic pressure. Figure 3 shows the estimation of the saddle loop flux Φ_{SL} and the diamagnetic flux Φ_{dia} with no toroidal current. Pressure profiles shown in Fig.3(a) and the toroidal flux Φ_0=3.144 (Weber) at 3T operation are used for calculations. As the pressure profile becomes more peaked, the saddle loop signal is larger, because P.S. current is larger as the gradient of pressure is larger. While the diamagnetic loop is not sensitive to the pressure profile.

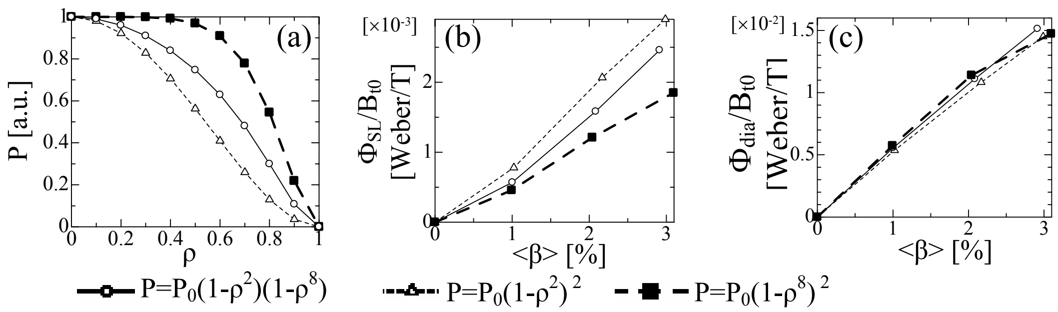

Fig. 3 (a)Pressure profile used this analysis. (b)The dependence of Φ_{SL} on pressure profiles with Φ_0=3.144 [Weber], where ρ is a normalized minor radius and B_{t0} is magnetic field strength at magnetic axis in the vacuum filed. (c) The dependence of Φ_{dia} on that.

4. Experimental result

Figure 4 shows time evolutions of Φ_{dia}, Φ_{SL}, the electron stored energy W_{pe} by profile measurements which are Thomson scattering and FIR laser interferometer, the line averaged electron density $\bar{n}_e$ and NBI power. In Fig. 5, we show the electron pressure profile measured by profile measurements at 1075, 1625, 2025 (msec) and the model pressure profile with the parabola $P=P_0(1-\rho^2)(1-\rho^8)$ and the broad $P=P_0(1-\rho^6)^2$. Figure 6 shows the experimental time trace of Φ_{dia} and Φ_{SL}. Green lines denote the relationships between Φ_{dia} and Φ_{SL} by calculations. From these figures, the experimental pressure profiles are between a parabolic model and a broad model and do not change so much on the time, but the ratio of Φ_{dia} and Φ_{SL} experimentally observed changes significantly. In the density-increase phase (a $\rightarrow$ b), we can see that Φ_{SL}/Φ_{dia} decreases. In the density-decrease phase(b $\rightarrow$ c), it increases. After NBI #1 off (c$\rightarrow$d), W_{pe} and Φ_{dia} do not change so much while Φ_{SL} decreases. Φ_{SL}/Φ_{dia} has a strong correlation with $\bar{n}_e$.

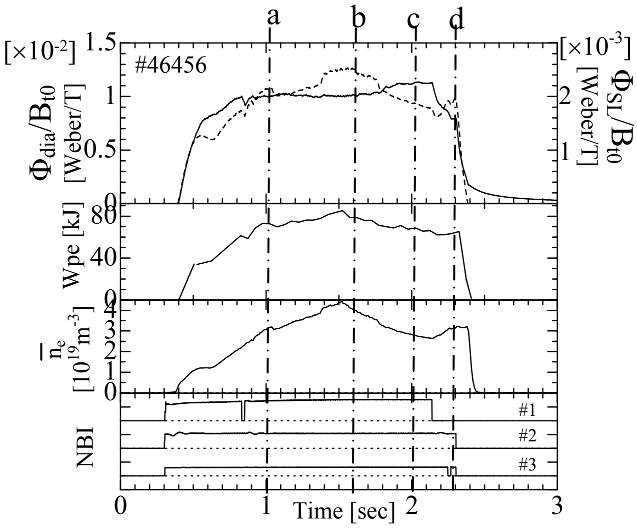

Fig. 4 Time evolutions of Φ_{dia}, Φ_{SL} and key parameters.

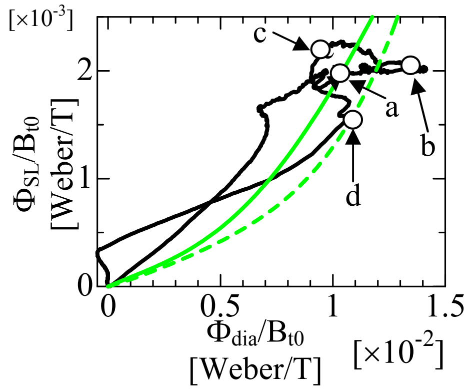

Fig.6 The time trace of measured Φ_{dia}, Φ_{SL} and isotropic estimations.

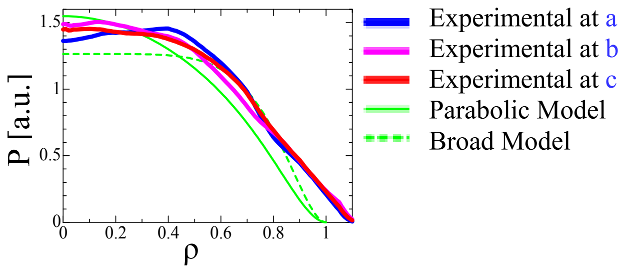

Fig. 5 The time evolution of pressure profile.

Figure 7 shows the relationship of measured Φ_{dia} and Φ_{SL} in many discharges where $\bar{n}_e$ are lager than $1\times10^{19}m^{-3}$ and B_{t0} are 0.5, 0.75 and 1.5T. And, the Φ_{dia} and Φ_{SL} calculated by VMEC-DIAGNO are shown under the assumption of parabolic and broad pressure profile models. We can see the strong correlation between Φ_{dia}/Φ_{SL} and $\bar{n}_e$, a higher density leads to a low value of Φ_{dia}/Φ_{SL}, in many discharges. In Fig.8, we show the comparison between the pressure anisotropy estimated by saddle loop fluxes and that by beam calculations due to NBI. Here we consider the following parameters; the pressure anisotropy estimated by saddle loops, $\Phi_{SL}^{exp}/\Phi_{SL}^{iso}$, and that estimated based on the beam calculation and diamagnetic measurements, W^{total}/W_{dia}. Here Φ_{SL}^{exp} is the measured saddle loop flux, Φ_{SL}^{iso} is VMEC-DIAGNO estimation under the assumption of parabolic pressure profile model, W_{dia} is the stored energy measured by the diamagnetic flux loop and W^{total} is the total energy. We assume $W_{dia}=W^{thermal}+1.5\,W_{\perp}^{beam}$, where $W^{thermal}$ is the thermal energy and $W_{\perp}^{beam}$ is the perpendicular component of the beam energy. Then, W^{total} is given by

$$W^{total} = W^{thermal} + W_{\perp}^{beam} + W_{\parallel}^{beam} = W_{dia} - 0.5W_{\perp}^{beam} + W_{\parallel}^{beam} \quad (1)$$

where $W_{\parallel}^{beam}$ is the parallel component of the beam energy. $W_{\perp}^{beam}$ and $W_{\parallel}^{beam}$ are calculated by a three-dimensional Monte Carlo simulation code [6]. The dependence of $\Phi_{SL}^{exp}/\Phi_{SL}^{iso}$ on $\bar{n}_e$ is consistent with that of W^{total}/W_{dia}. We consider that $\Phi_{SL}^{exp}/\Phi_{SL}^{iso}$ detects the pressure anisotropy, because the parallel component of NBI power is dominant in LHD and the beam contribution to pressure is large anisotropy in low density.

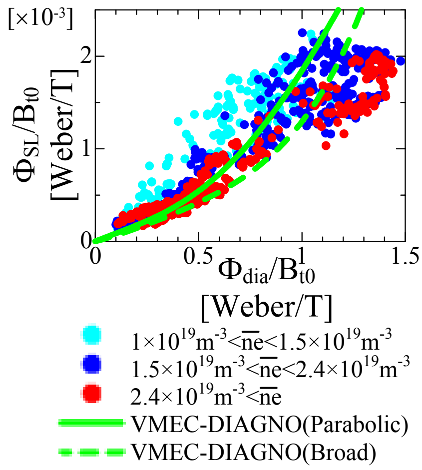

Fig. 7 The dependence of Φ_{dia} and Φ_{SL} on $\bar{n}_e$.

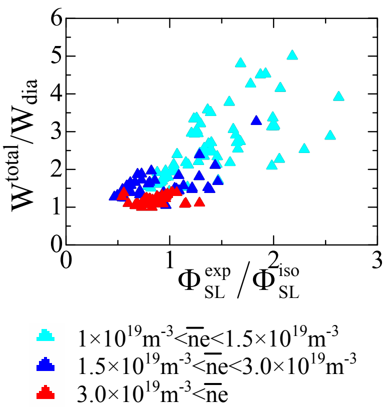

Fig. 8 The comparison between $\Phi_{SL}^{exp}/\Phi_{SL}^{iso}$ and W^{total}/W_{dia}.

5. Summary

The experimental time trace of Φ_{dia} and Φ_{SL} is not consistent with VMEC-DIAGNO calculation when the isotropic pressure is assumed. The ratio between experimental saddle loop flux and isotropic estimation depends on $\bar{n}_e$ and it is consistent with the beam energy calculation due to NBI. We have confirmed that the diamagnetic loop and the saddle loop has a capability to measure the pressure profile and the pressure anisotropy in LHD. We need more analyses to quantitatively evaluate the pressure profile and the pressure anisotropy.

References

[1] S. Morimoto, et al., Nucl. Fusion **28**, 1491 (1988).

[2] J. Qin, et al., Nucl. Fusion **36**, 381 (1996).

[3] A. Iiyoshi et al., Nucl. Fusion **39**, 1245 (1999).

[4] S. P. Hirshman and W. I. van Rij, Comput. Phys. Commun. **43**, 143 (1986).

[5] H. J. Gardner, Nucl. Fusion **30**, 1417 (1990).

[6] S. Murakami, N. Nakajima and M. Okamoto, Trans. Fusion Technol., 27, 256 (1995).